Hindawi
Shock and Vibration
Volume 2020, Article ID 8830371, 13 pages
https://doi.org/10.1155/2020/8830371

*Research Article*

# The Properties of a Coal Body and Prediction of Compound Coal-Rock Dynamic Disasters

**Guowei Dong**,[1,2,3] **Xuanming Liang**,[1,3] **and Zhen Wang**[4,5]

[1]*School of Energy Engineering, Xi'an University of Science and Technology, Xi'an 710054, China*
[2]*The State Key Laboratory of Coal Resources and Safe Mining (CUMT), Xuzhou 221116, China*
[3]*Key Laboratory of Western Mine Exploitation and Hazard Prevention of the Ministry of Education, Xi'an 710054, China*
[4]*China Coal Technology and Engineering Group Corp Chongqing Research Institute, Chongqing 400039, China*
[5]*National Key Laboratory of Gas Disaster Monitoring, Preventing and Emergency Controlling, Chongqing 400039, China*

Correspondence should be addressed to Guowei Dong; leng285@xust.edu.cn

Received 30 April 2020; Revised 28 June 2020; Accepted 27 July 2020; Published 20 August 2020

Academic Editor: Caiping Lu



Since the precise identification and prediction and early warning of compound coal-rock dynamic disaster remain difficult, a new coal characterisation and prediction method for compound coal-rock dynamic disasters was described based on theoretical analysis, laboratory experiment, field sampling, mathematical treatment, and industrial testing. The results implied that the physicomechanical properties of coal in a compound coal-rock dynamic disaster are between those pertinent to a typical rock burst and a coal-gas outburst, i.e., with high crustal stress surrounding pressure, high gas pressure, low permeability, bump proneness, and outburst risk. The predicted drilling data indicate moderate gas desorption indices. The gas desorption velocity and permeability of compound coal-rock dynamic disaster coal decrease with the increase in crustal stress, while increase and decrease with the increase in gas pressure, respectively, at the same time, and they change little with increasing temperature. Gas extraction leads to the increase in coal mass brittleness and bump proneness. Based on the unique physical-mechanical properties of compound coal-rock dynamic disaster coal, a reasonably sensitive predictive index and critical value for Donglin Coal Mine were determined.

## 1. Introduction

Due to the prevailing demand for energy resources, the coal-based energy pattern of China will not change in the foreseeable future. The proportion of coal in the energy system will remain at around 50% in the long-term, and 80% of coal is mined from a deeper underground, especially in mideastern China. Due to deep mining, the features of coal-rock dynamic disasters become more complicated and diverse; thereby, a new compound coal-rock dynamic disaster occurs. Besides, in some middeep regions with abnormal gas geology, new compound coal-rock dynamic disasters also occur. This new compound coal-rock dynamic disaster presents a dual dynamic feature combining bump proneness and outburst risk; that is, the disaster exhibits the features of both typical coal-gas outburst and rock burst (Figure 1).

In recent years, some of China's coal mines such as those in the Pingdingshan mining areas, Huainan mining areas, Xinji mining areas, Fengcheng mining areas, Fuxin mining areas, and Fushun mining areas took the lead in deep mining, where some compound coal-rock dynamic disasters already occurred or are likely to occur.

At present, many scholars have studied the mechanism of compound coal-rock dynamic disasters, their prediction, early warning, and prevention: Petukhov [1], Zhang et al. [2], He et al. [3], Li et al. [4, 5], Li [6], Zhang et al. [7], Pan [8], Yin et al. [9], Dou et al. [10], and Dong et al. [11] have studied the occurrence mechanism of compound coal-rock dynamic disaster. Zhang and Li [12], Zhen et al. [13], Li et al. [14], Yuan [15], Li et al. [16], Qi et al. [17], Pan [8], Yin et al. [9], and Dou et al. [10] studied the occurrence conditions or types of compound coal-rock

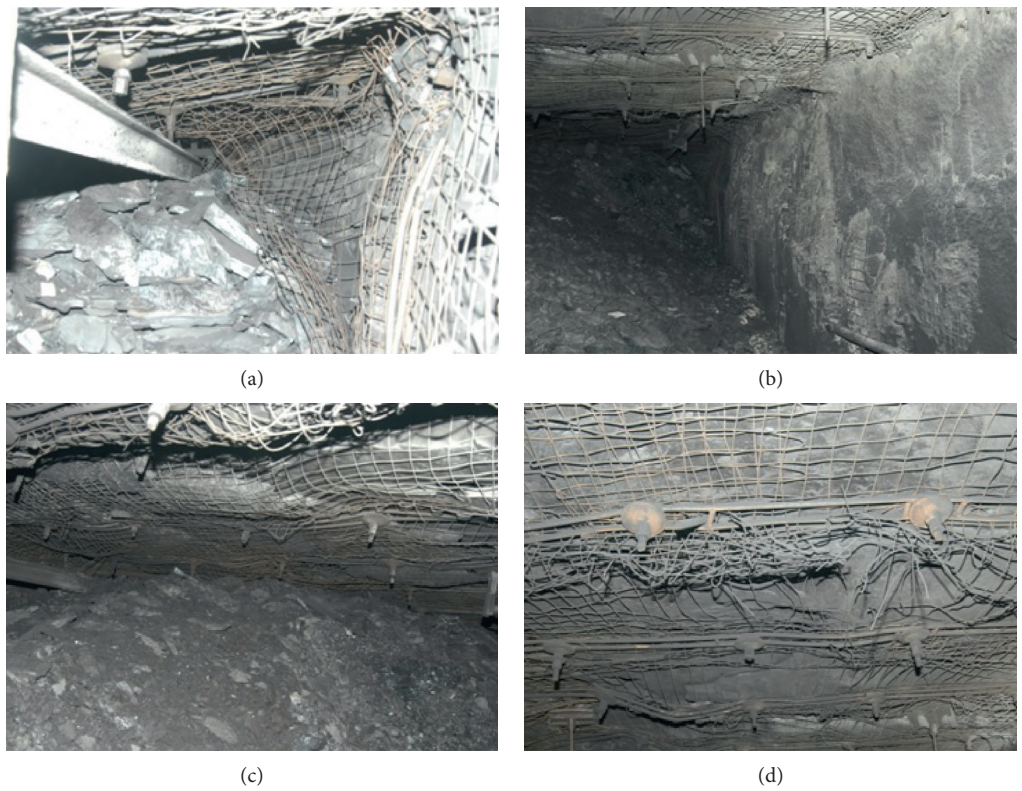

Figure 1: A compound coal-rock dynamic disaster accident: no. 12 coal mine, Pingdingshan Coal Group Co., Ltd.: (a) damage on the roadway supports; (b) the piling of coal flow; (c) the piling of coal flow; (d) normal supports of roadway.

dynamic disasters. Zhang [18], Yuan [15], Jianwei [19], Jiang et al. [20], Dong et al. [11], Sheng et al. [21], and Ouyang et al. [22] have studied the prediction, early warning, and evaluation of compound coal-rock dynamic disasters. Qi et al. [23] investigated the theory and technical framework of multiscale and multisource prevention and control of coal-rock dynamic disasters in deep coal mines. The prediction and early warning of a compound coal-rock dynamic disaster mainly relies on the direct or indirect parameters such as the amount of drilling cuttings [5–7, 10, 11, 15, 18, 20, 21, 23, 24], the size of the drilling cuttings [8, 23], the temperature of the drilling cuttings [8, 23], the desorption index of the drilling cuttings [5, 7, 11, 15, 18], the initial velocity of gas emission from boreholes [5, 7, 10, 11, 15, 18], the stress [7, 19, 20, 23], the displacement [23], the gas concentration extraction index [11, 20], coal temperature [8], coal charge [8], electromagnetic radiation [10], microseismic event count [10, 19, 20, 23, 25], acoustic emission event count [10, 11, 20, 21], shock wave CT [10], and seismic wave or elastic wave CT [10, 23]. However, the coal physical-mechanical characterisation and prediction method of a compound coal-rock dynamic disaster still contain many deficiencies; therefore, in this study, a new coal characterisation and prediction method of compound coal-rock dynamic disasters were studied, based on the actual occurrence data of compound coal-rock dynamic disasters.

## 2. Physicomechanical Properties of Coal in a Compound Coal-Rock Dynamic Disaster

### 2.1. Physical Properties

*2.1.1. Experimental Study of the Coal-Gas Desorption Regularity of Compound Coal-Rock Dynamic Disaster.* The instantaneous desorption (from the initial desorption to steady state) features of gas in coal samples after artificial unloading under different mining conditions were analysed via laboratory experiments. These experimental results are the foundation for the further study of different action mechanisms of stress, gas, and temperature on the risk of a disaster occurring.

Under certain confining pressure (CP) and gas pressure (GP) conditions, the desorption features of gas at different temperatures were analysed to reveal the controlling effect of temperature on gas desorption. Under a specific confining pressure and temperature conditions, the influence of gas pressure on the coal desorption regularity was discussed. The influence of confining pressure on the gas desorption behaviour was also studied under specific pore pressure and temperature conditions.

During the experiment, the Darcy steady flow method and triaxial penetration test device were used. The outlet pressure is the atmospheric pressure, while the inlet pressure is adjustable. The desorption and penetration experiments of coal samples under different gas pressures, temperatures,

and confining pressure conditions were conducted. The main device and experimental system used are displayed in Figure 2.

By using a customised rock coring and detection device, the raw coal was cut into cylinders measuring Φ50 mm × 100 mm. After that, the samples were ground using an electric grinder, to meet test requirements. Experimental results and trend analyses are demonstrated in Figures 3–6.

(1) Variation regularity of raw coal-gas desorption velocity (GDV) with confining pressure

The gas desorption velocity curves under different confining pressures are shown in Figure 3. During the test, the gas adsorption pressure is 2 MPa, and the temperature is 35°C. As shown in Figure 3, when the confining pressure is 6 MPa, the gas desorption velocity is greater than those under confining pressures of 10 and 12 MPa, in both the initial stage and steady stage. Meanwhile, the gas desorption velocities under confining pressures of 10 MPa and 12 MPa remain similar.

As shown in Figure 4, when the confining pressure increases from 6 to 8 MPa, the gas desorption velocity (after entering the steady stage) sharply decreases from 2.72 to 1.51 $cm^3/s$. Meanwhile, the gas desorption velocities at 10 MPa and 12 MPa are 1.31 $cm^3/s$ and 1.22 $cm^3/s$, respectively. That is, under specific gas pressure and temperature conditions, the influence of confining pressure on the gas desorption velocity decreases gradually, after it increases to a certain value.

(2) Variation in raw coal-gas desorption velocity with gas adsorption pressure

The gas desorption velocity curves under different gas pressures are shown in Figure 5. During the test, the confining pressure is 6 MPa, and the temperature is 35°C. As displayed in Figure 5, when the gas adsorption pressure reaches 4 MPa, the gas desorption velocity is beyond the range of the instrumentation used, so its values are not illustrated in the figure. Hence, no matter in the initial stage or the steady stage, the gas desorption velocity increases with the improvement of gas adsorption pressure.

(3) Variation in raw coal-gas desorption velocity with temperature

The gas desorption velocity curves under different temperature conditions are shown in Figure 6. During the test, the gas adsorption pressure is 1 MPa, and the confining pressure is 6 MPa. As illustrated in Figure 6, in the initial stage, the raw coal-gas desorption velocity at low temperatures is higher than that at high temperatures. Meanwhile, the final desorption velocity at low temperatures is lower than that at high temperatures.

*2.1.2. Experimental Study of the Coal-Gas Permeability in a Compound Coal-Rock Dynamic Disaster.* The variation in coal permeability (gas permeability coefficient) under different conditions was characterised. The main device and experimental system used are displayed in Figure 2.

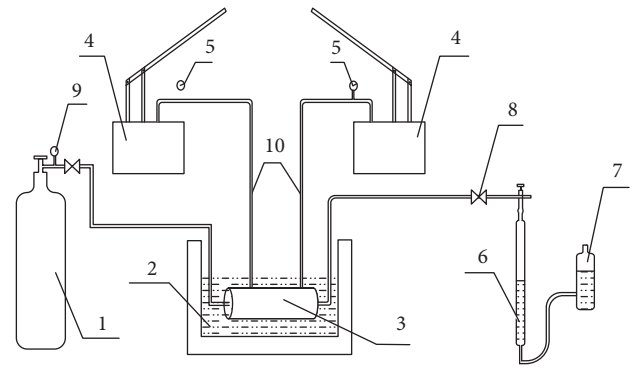


Figure 2: Schematic of the experimental system. 1, high-pressure gas cylinder; 2, thermostatic water bath; 3, triaxial osmoscope; 4, manual hydraulic pump; 5, oil pressure gauge; 6, burette; 7, levelling bottle; 8, valve; 9, reducing valve; 10, hydraulic tube.

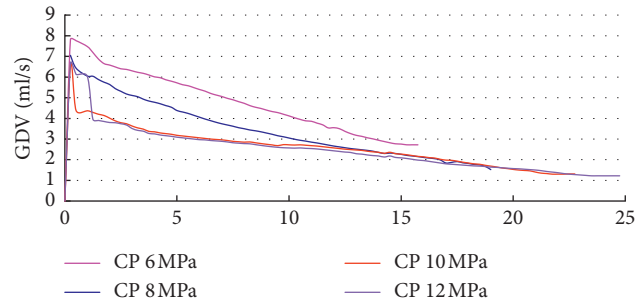


Figure 3: Gas desorption velocity curves under different confining pressure conditions.

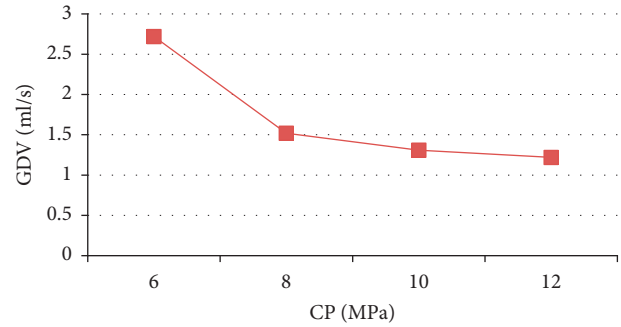


Figure 4: Change in gas desorption velocity with confining pressure.

(1) Variation in raw coal permeability with changing confining pressure

The variation in permeability during continuous unloading is shown in Figures 7–10. As shown in the figure, the coal permeability gradually increases during unloading and the rate of increase also increases. In the initial unloading stage, i.e., high confining pressure stage (high burial depth), the

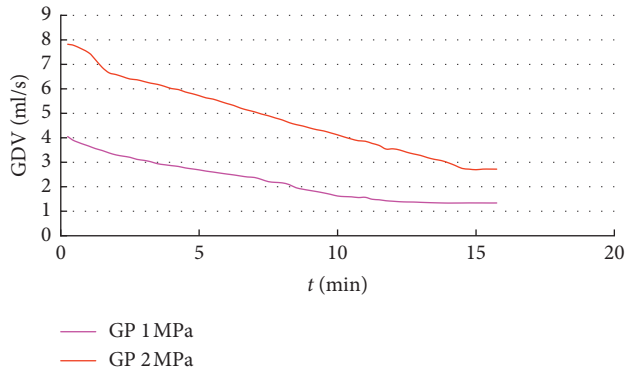


Figure 5: Gas desorption velocity under different gas pressure conditions.

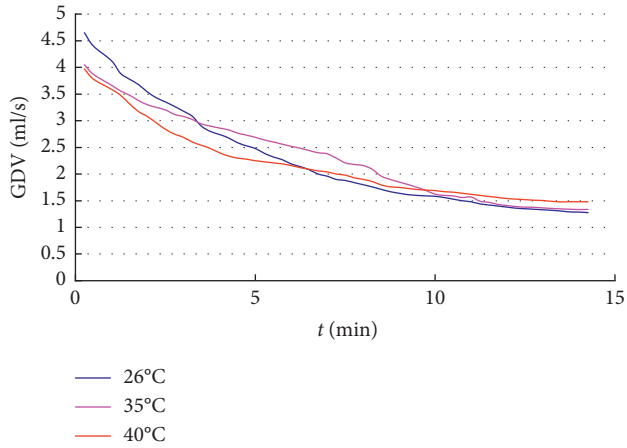


Figure 6: Gas desorption velocity curves under different temperature conditions.

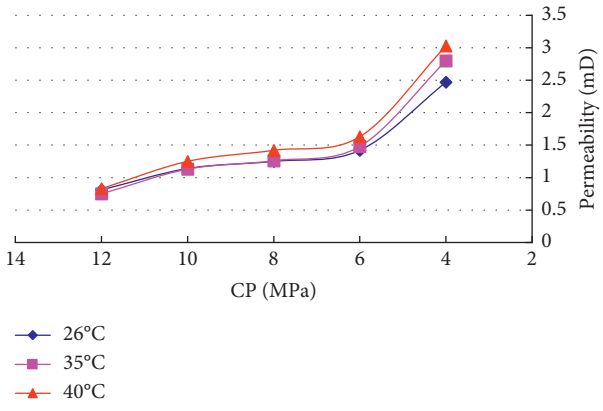


Figure 7: Variation in permeability during confining pressure unloading at a gas pressure of 1 MPa.

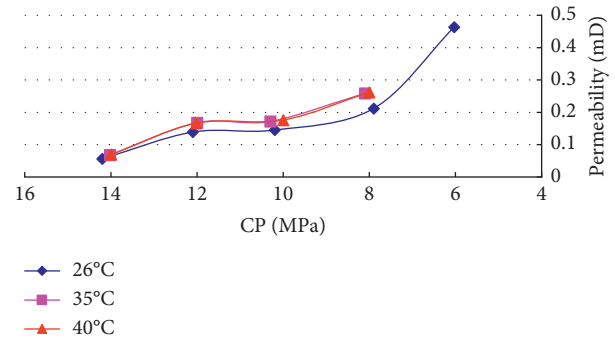


Figure 8: Variation in permeability during confining pressure unloading at a gas pressure of 4 MPa.

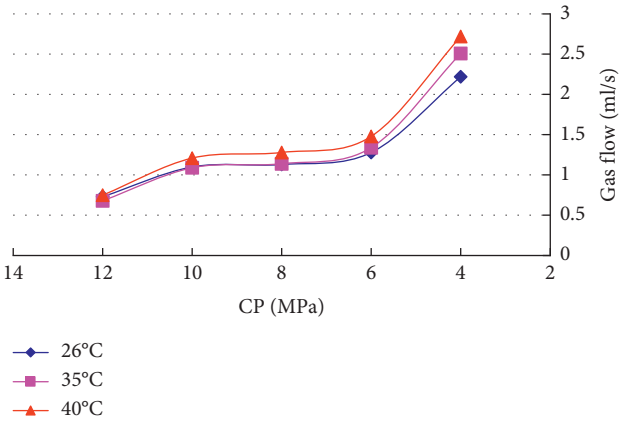


Figure 9: Variation in gas flow during confining pressure unloading at a gas pressure of 1 MPa.

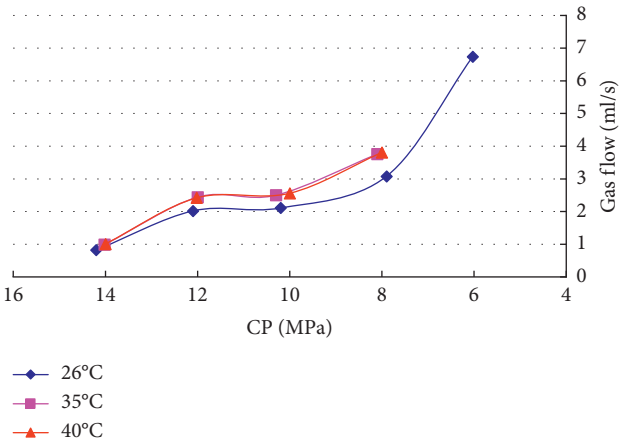


Figure 10: Variation in gas flow during confining pressure unloading at a gas pressure of 4 MPa.

permeability rises slowly during the unloading of confining pressure. Meanwhile, in the mid-late stage, i.e., low confining pressure stage (low burial depth), the increase rate of coal permeability is accelerated during unloading. For example, when the adsorption pressure is 1 MPa, the rate of increase increased under confining pressures is lower than 6 MPa. Meanwhile, when the adsorption pressure is 4 MPa, the rate of increase rate is increased under confining pressures is lower than 8 MPa. In a word, the variation in permeability is closely related to the initial confining pressure (burial depth or tectonic stress) and gas pressure.

According to the above analysis, when the adsorption pressure and temperature are constant, upon the reduction of confining pressure, the permeability increases gradually; in the initial stage of unloading, i.e., the high confining pressure stage, the increasing amplitude of permeability is relatively small; meanwhile, in the later stage of unloading, i.e., the low confining pressure stage, the rate of increase of permeability is increased; the gas flow changes in a way similar to the permeability.

(2) Variation in raw coal permeability with gas pressure changing

The permeability of the same sample under different gas adsorption pressures was characterised. The results indicate that, with the increase in gas adsorption pressure, the permeability decreases. On the contrary, the gas desorption velocity; i.e., the gas flow increases accordingly (Figures 11 and 12).

(3) Variation in raw coal permeability with changing temperature

Figures 13–15 show the variation between the sample permeability and temperature under different confining pressures when the gas adsorption pressure is 1 MPa and 4 MPa, respectively. As shown, the coal permeability increases with increasing temperature because as the temperature rises, the activity and internal energy of gas molecules increase. Some of the adsorbed gas is desorbed. The seepage channels expand. The diffusion of gas molecules is accelerated; thus, the permeability of coal gas increases accordingly.

Under high confining pressure conditions, the increase in permeability with temperature is relatively small yet becomes more significant at low confining pressure. In particular, when the gas adsorption pressure is 4 MPa, the seepage flow velocity exceeds the measuring range of equipment and cannot be precisely determined.

According to the above analysis, when the adsorption pressure and confining pressure are constant, with the increase in temperature, the coal permeability rises slightly, but the variation is smooth (Figures 13 and 14); under high confining pressure, the increase in permeability as the temperature rises is relatively small (a trend that strengthens under low confining pressure conditions, as shown in Figure 14); when the gas adsorption pressure is 4 MPa, the seepage flow velocity and permeability (confining pressure of 6 MPa and temperatures of 35°C and 40°C) exceed the measuring range of equipment and cannot be accurately measured. Meanwhile, Figure 15 indicates that the variation in gas flow is similar to that of the permeability.

*2.2. Coal Mechanical Properties in a Compound Coal-Rock Dynamic Disaster.* By using gas-tight equipment [26], the approximate-uniaxial test method for the characterisation of gas-containing coal mechanical properties was developed.

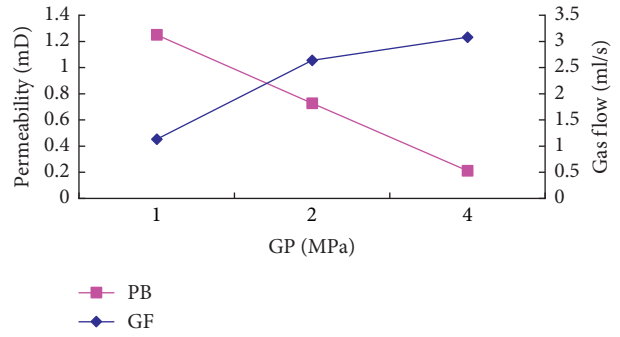


Figure 11: At 26°C.

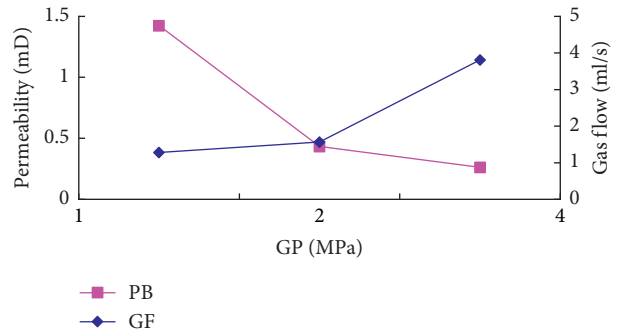


Figure 12: At 40°C.

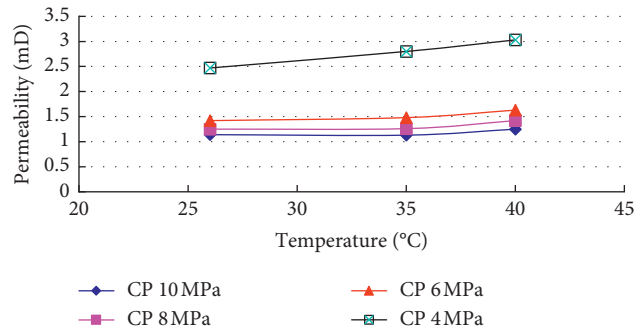


Figure 13: Variation in permeability with increasing temperature at a gas pressure of 1 MPa.

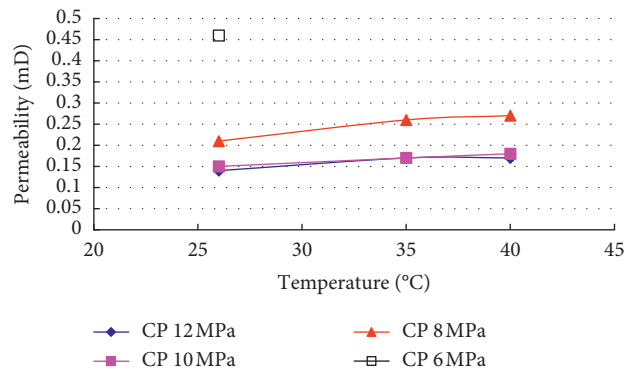


Figure 14: Variation in permeability with increasing temperature at a gas pressure of 4 MPa.

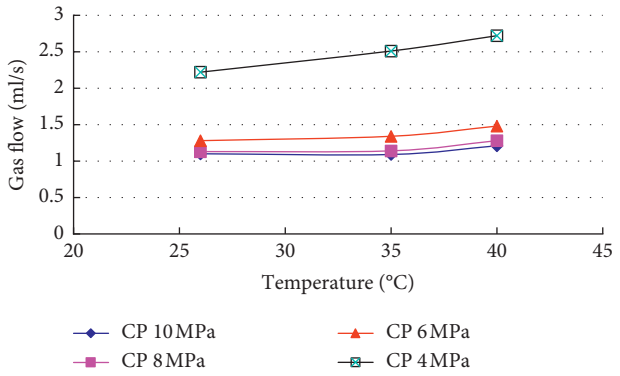


Figure 15: Variation in gas flow with increasing temperature at a gas pressure of 1 MPa.

Based on experiment, the influence of gas on the coal mechanical properties and mechanical response under zero effective confining pressure condition was obtained.

*2.2.1. Stress-Strain Curves of Coal Samples under Uniaxial Compression.* In uniaxial compression tests, the gas pressures were set to 0 MPa, 1 MPa, and 2 MPa, respectively. Under each condition, at least three samples were characterised. The experimentally obtained stress-strain curves and related data are displayed in Figures 16 and 17.

Figure 16 shows the uniaxial compression stress-strain curve of coal samples without gas being present. As shown in the figure, although the samples are cut from the same coal block, the uniformity of bedding direction is ensured, so some discreteness of measured data is unavoidable. Figure 17 demonstrates the stress-strain curves of coal samples uniaxially compressed under various gas pressure conditions. The gas in pores and fissures not only changes the mechanical properties and mechanical response of the coal body in the plastic deformation stage and after peak strength deformation stage but also affects the elastic deformation of the coal body; i.e., mechanical properties such as elastic modulus no longer remain constant. In other words, the gas pressure changes the mechanical response features of coal in all deformation stages, including its elastic deformation stage.

*2.2.2. Influence of Adsorbed Gas on Coal Mechanical Properties.* Within the coal, gas exists in the free and adsorbed states. Under specific temperature and pressure conditions, a dynamic equilibrium is reached. The physicomechanical properties of coal containing gas are affected by these two gas states. The free gas affects the mechanical properties of coal via pore pressure which affects the volumetric strain. Meanwhile, adsorbed gas changes the mechanical properties and mechanical response of coal via the adsorption and desorption processes, which further affect the constitutive relationship of the coal.

(1) Elastic modulus (EM) decreases with the increase in gas pressure

As shown in Figure 18, the elastic modulus decreases with the increase in gas pressure. Gas molecules adsorbing on the coal particle surface and interparticle space will reduce the cohesion of the coal samples, so the macroscopic deformation resistance of coal sample is decreased; i.e., the elastic modulus is reduced.

(2) Plastic deformation at the peak point decreases with the increase in gas pressure

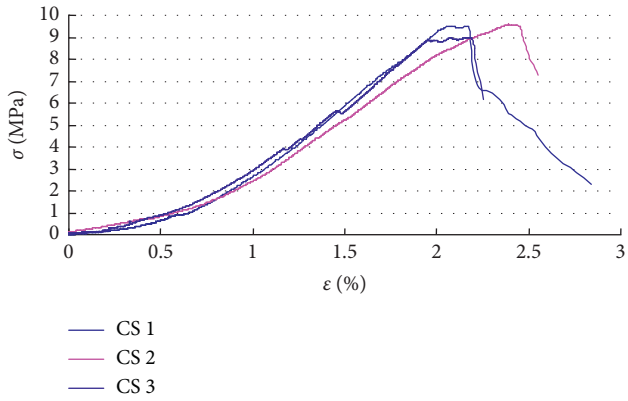


Figure 16: Stress-strain curves of coal samples (CS) compressed under no-gas conditions.

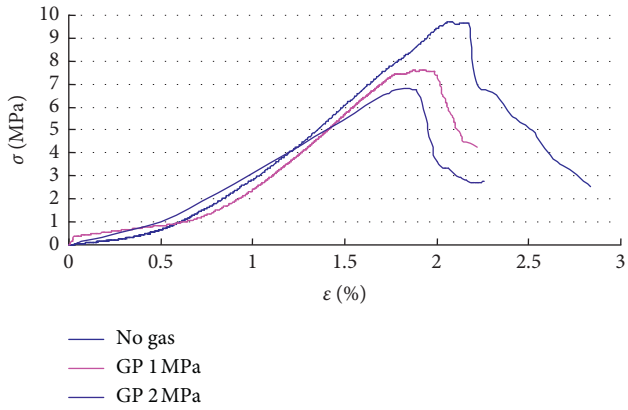


Figure 17: Stress-strain curves of coal samples compressed under different gas conditions.

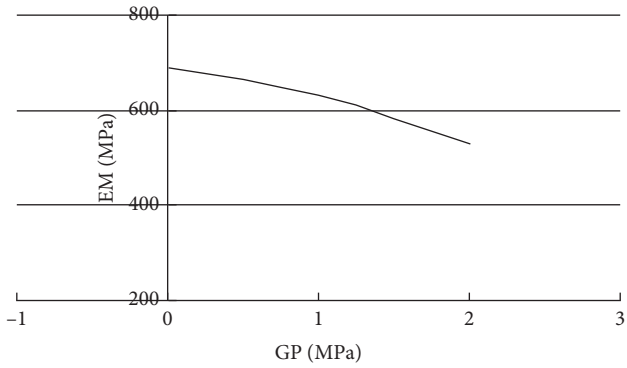


Figure 18: Variation in elastic modulus with changing gas pressure.

As shown in Figure 19, at the peak point stage, the plastic deformation of coal sample gradually decreases with the increase in gas pressure.

(3) Influence of gas on the bump proneness index

Experimental results of coal bump proneness index under different gas pressures are listed in Table 1.

As shown in Figure 20, the dynamic fracture time, i.e., the time required for the occurrence of brittle fracture, increases with the increase in gas pressure.

The bump energy index and elastic energy index both decrease with the increase in gas pressure. Comparing to coal body skeleton frame bearing load alone, the coal body skeleton frame and gas bear the external load together after gas adsorption. Thus, the elastic deformation energy accumulated within the coal body is significantly reduced, making it difficult for the formation of coal body bump burst. Besides, according to the method used for calculation of bump energy index and elastic energy index, the reduction of uniaxial compressive strength and elastic modulus will result in the reduction of bump energy index and elastic energy index with the increase in gas pressure, as shown in Figures 21 and 22.

Based on above analyses, as the mine gets deeper, the gas extraction is likely to increase the bump proneness of coal with the increase in coal strain energy. Thus, the risk of compound coal-rock dynamic disaster is increased.

(4) Brittleness decreases with the increase in gas pressure

As shown in Figures 16 and 17, the presence of gas makes the postpeak curve more shallow; in particular, the brittle fracture, that stage with a sharp instant reduction in strength, is less significant. This is mainly attributed to the existence of gas increasing the ductility of coal and reduces the possibility of brittle fracture. As shown in Figure 23, after the fracture of samples without gas adsorption effect, the sample fractures into a relatively complete split line; meanwhile, for samples affected by gas adsorption, they fragment, exhibiting poor completeness after fracture.

Also, it can also be found that the trend in coal mechanical properties and mechanical response slows as the gas pressure increases. In other words, under the uniaxial compression condition with zero confining pressure, the influence of gas on the coal mechanical properties and mechanical response gradually diminishes when the gas adsorption reaches saturation. Gas extraction will increase the risk of compound a coal-rock dynamic disaster.

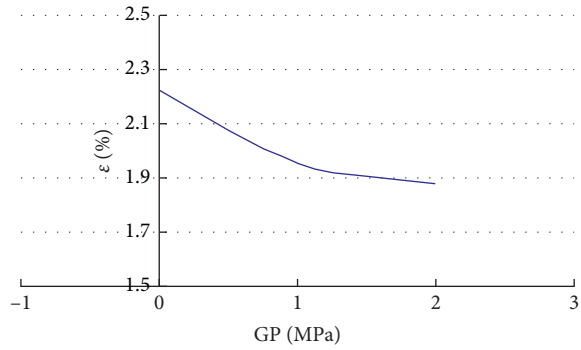


Figure 19: Variation in peak point plastic deformation for changing gas pressure.

## 3. Prediction Used in a Case Study of a Compound Coal-Rock Dynamic Disaster

*3.1. Mine Overview: Contorted Fold Structure Characteristics and Compound Coal-Rock Dynamic Disaster Condition of Donglin Coal Mine.* Donglin Coal Mine is located in Wansheng District, Chongqing City; it is a coal-gas outburst mine and adopts the vertical multilevel partition mining method. It mainly exploits the No. 4 and No. 6 coal seams in the Permian Longtan formation. The types of coal are coking coal, lean coal, meagre coal, and fat coal. Donglin Coal Mine lies along the Ganjiaping syncline shaft. Folds in the mine are classified as secondary folds of the Bamianshan syncline. Secondary tectonics include the Ganjiaping syncline, Maoyan anticline, Yaqueyan syncline, Heiqiyan torsion, and Yaqueyan torsion, as shown in Figure 24.

Contorted fold structures are folds transiting from normal incline to inverted incline or compress shear and noncylindrical folds caused by trend transition and increasing dip angle. According to the formation area and morphological features of contorted fold structures, the fold structures can be classified into reverse or kinked structures.

The Heiqiyan contorted fold band in Donglin Mine is distributed approximately north to south, with a total length of 4 km, and Heiqiyan Matong marks the transition point. Its south trend is 1.5 km. The deep stratum trend transits into S30°W, and the incline is W (i.e., the east wing of the Ganjiaping syncline); the band trend between the north of Matong and boundary is 2.5 km. The stratum overturns into an east incline of 30°. Its shallow seam trend is N10°W, while the deep seam trend is N10°E. The ground elevation is +310 m, and the production level is − 100 m. The initial crustal stress is 56.3 MPa. The initial gas pressure is 1.8 MPa. The initial bump proneness indices of coal seam are such that the dynamic fracture time DT is 323 ms, elastic energy index $W_{ET}$ is 2.16, bump energy index $K_E$ is 1.64, and the uniaxial compressive strength $R_c$ is 4.3 MPa, thus indicating bump proneness.

Donglin Coal Mine is located at the intersection of the north-east secondary fold and the north-south structure. Due to stress imbalance, contorted fold structures are formed in Heiqiyan.

During the formation of contorted fold structures in Donglin Coal Mine, severe damage to the coal body structure and intensive changes in coal attitude are caused by compression and interformational sliding. Furthermore, the contorted fold structures also form a closed structural unit with favourable gas occurrence: these geological factors lead to the serious compound coal-rock dynamic disaster accidents that have occurred in Donglin Coal Mine.

Table 1: Experimental results of coal bump proneness index under different gas pressure conditions.

| Type name | | 1-type without gas | 2-type gas pressure of 1 MPa | 3-type gas pressure of 2 MPa |
|---|---|---|---|---|
| Bump proneness index | Dynamic fracture time (ms) | 280 | 630 | 640 |
| | | 260 | 480 | 460 |
| | | 320 | 570 | 720 |
| | Average | 287 | 560 | 607 |
| | Elastic energy index (EEI) | 2.33 | 1.87 | 1.77 |
| | | 3.21 | 1.76 | 1.52 |
| | | 2.90 | 1.69 | 1.43 |
| | Average | 2.81 | 1.77 | 1.57 |
| | Bump energy index (BEI) | 1.92 | 1.62 | 1.23 |
| | | 1.74 | 1.51 | 1.35 |
| | | 1.81 | 1.38 | 1.56 |
| | Average | 1.82 | 1.50 | 1.41 |

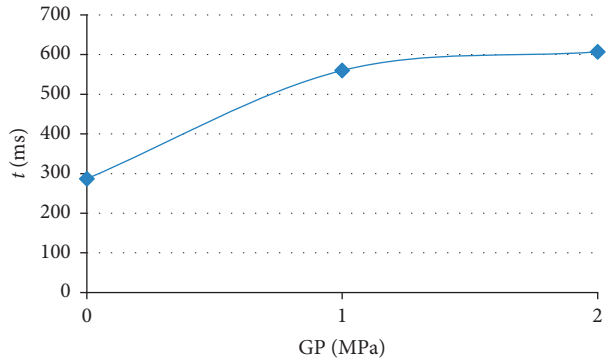


Figure 20: Variation in dynamic fracture time with changing gas pressure.

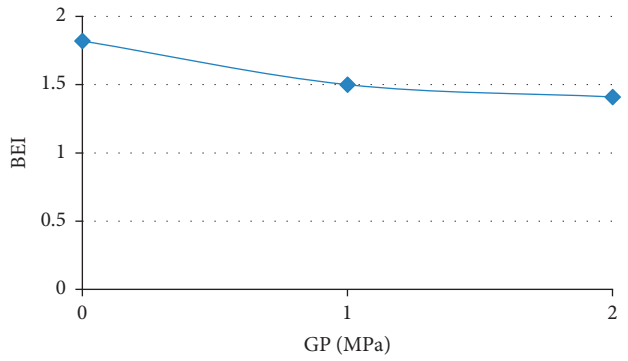


Figure 21: Variation in bump energy index with changing gas pressure.

To date, about 200 compound coal-rock dynamic disasters have occurred in Donglin Coal Mine, with an average intensity of 72.8 t each. The maximum intensity reached 3500 t, and the maximum gas emission was 200,000 $m^3$. Altogether, 92 people have died in such gas accidents. As for the No. 4 coal seam, the maximum intensity was 3500 t, while that for the No. 6 coal seam was 160 t. The parameters of compound coal-rock dynamic disasters in Donglin Coal Mine are summarised in Table 2.

*3.2. Study of the Prediction Index for Compound Coal-Rock Dynamic Disasters in Donglin Coal Mine.* In this study, the prediction indices of compound coal-rock dynamic disaster are studied mainly focusing on the No. 6 coal seam in the north wing of Donglin Coal Mine, via laboratory tests and field investigation.

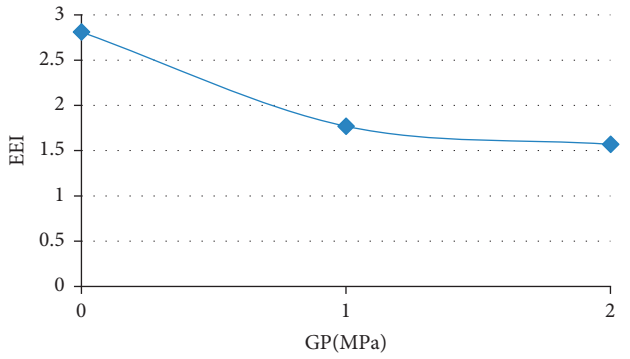


Figure 22: Variation in elastic energy index with changing gas pressure.

*3.2.1. Laboratory Study.* Soft coal samples were collected in the 2607-50 heading face and 2609-90 heading face. Risk parameters of compound coal-rock dynamic disaster were measured in the laboratory, with the results listed in Table 3. In the table, 0.5 MPa, 0.74 MPa, and 1.1 MPa are the assumed gas pressures used.

The risk parameters of a compound coal-rock dynamic disaster include initial gas emission velocity $\Delta P$ and the consistency coefficient of coal $f$. The $K_1$-$P$ relationship was fitted according to related experimental data. As shown in Table 3, coal samples were collected at different sites in the No. 6 coal seam. The critical value of $K_1$ was determined to be 0.10 to 0.23 based on the minimum gas pressure method. The gas parameters and mechanical parameters of compound coal-rock dynamic disaster were mainly decided by laboratory investigation. The critical gas desorption index $K_1$ was determined based on the critical gas pressure of 0.74 MPa and the theoretical gas pressure of 1.1 MPa calculated according to the consistency coefficient.

*3.2.2. Field Investigation.* Some 70 prediction cycles were carried out in the 2607-50 heading face and 2609-90 heading

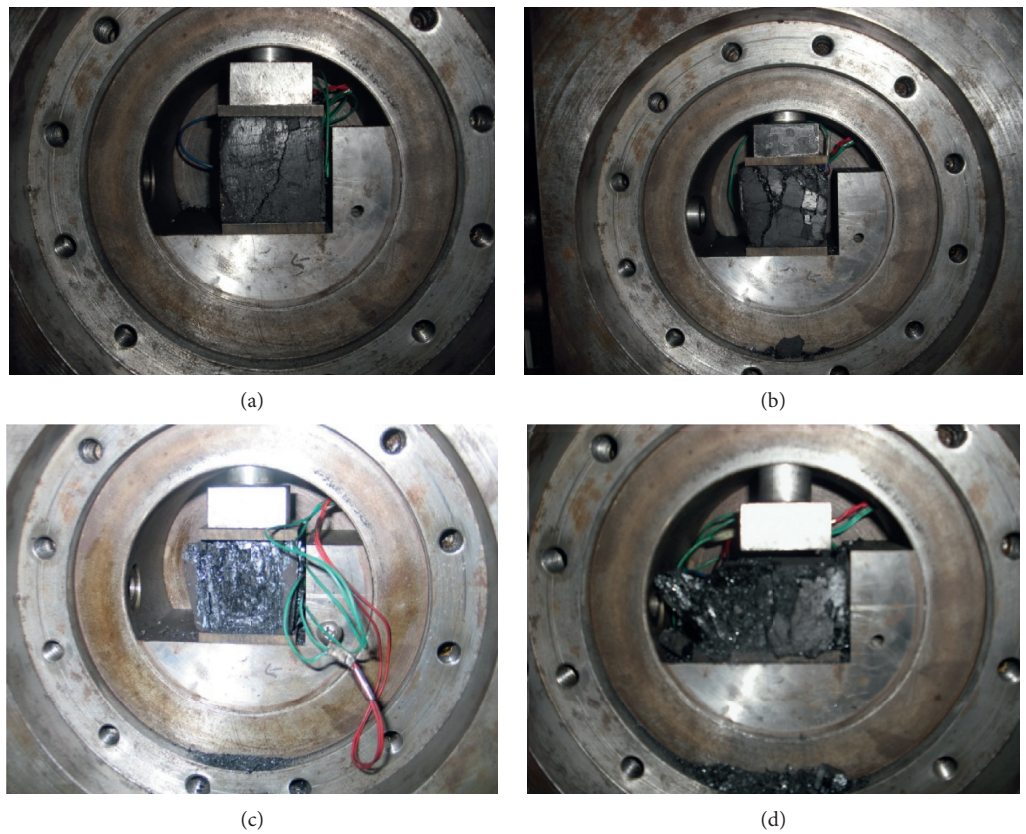

(a) (b) (c) (d)

Figure 23: Fracture patterns of coal samples compressed under different gas pressures: (a) without gas effect; (b) under the influence of 1 MPa gas pressure; (c) under the influence of 2 MPa gas pressure.

face during the study, with 58 sets of prediction data collected.

Among the 58 sets of data, on more than 26 occasions, the prediction rate of compound coal-rock dynamic disaster reached 45%. The averaged maximum values of $K_1$ and $S$ in the 58 sets of data are 0.16 ml/g·min$^{1/2}$ and 14.3 kg/m, respectively. A check on the result cycle was conducted after 25 events (i.e., a check rate of 32%). The per-metre cuttings desorption index of prediction cycle, and the distribution of the maximum prediction cycle and check cycle values of this index, is listed in Tables 4–6, corresponding to Figures 25–28.

According to Tables 4 and 5, the maximum average value of per-metre drilling index $K_1$ is 0.08 ml/g·min$^{1/2}$, while the maximum average value of $S$ is 8.2 kg/m.

Based on the above field measurements, it is implied that the following relationship exists between the desorption index of cuttings, kinetic phenomena, hole depth, and coal seam occurrence: for $K_{1\max} < 0.2$, no spray hole phenomenon has been reported. When the coal body is relatively hard (failure type II and consistency coefficient of 0.7) and no drill jamming or coal-gunning occurs, the maximum drilling chip amount index $S$ is usually around 6.0 kg/m. When the coal body is relatively hard (failure type II and firmness of 0.7) and there is drill jamming or coal-gunning, the maximum drilling chip amount index $S$ is usually above 15 kg/m. For soft coal (failure types III and IV and consistency coefficient of 0.2) with drill jamming or coal-gunning, the maximum drilling chip amount index $S$ is even greater.

The prediction or check cycle drill hole depth should be controlled to within 10 m; the maximum drilling chip amount index $S$ occurs within a hole depth of 6 m, so the maximum index $K_1$ value occurs within a hole depth of 9 m.

In areas with significant coal seam occurrence (average seam thickness) variation, hole collapse, drill jamming, and coal-gunning occur frequently.

In ordinary mines, the occurrence rate of compound coal-rock dynamic disaster is between 5% and 10%. By considering a safety factor of three, the critical value of the compound coal-rock dynamic disaster prediction was theoretically determined; i.e., the number of an index exceeding a certain value accounts for 30% of the total number of statistical items of data. As shown in Table 6 and Figures 27 and 28, the ranges of different $K_1$ and $S$ were obtained via statistical analysis of data obtained through 58 field tests.

According to the range of $K_{1\max}$ obtained via 58 field tests, the maximum value of $K_1$ exceeding 30% is 0.2 mL/(g·min$^{1/2}$), the proportion of which is 31% overall. As implied by field investigation results, when $K_1 < 0.2$ mL/(g·min$^{1/2}$), no spray hole phenomenon has been reported. With the increase in $K_1$, the possibility of occurrence of kinetic phenomena including spray hole development increases.

According to the range of the prediction cycle drilling chip amount index $S_{\max}$ obtained through 58 field tests, the

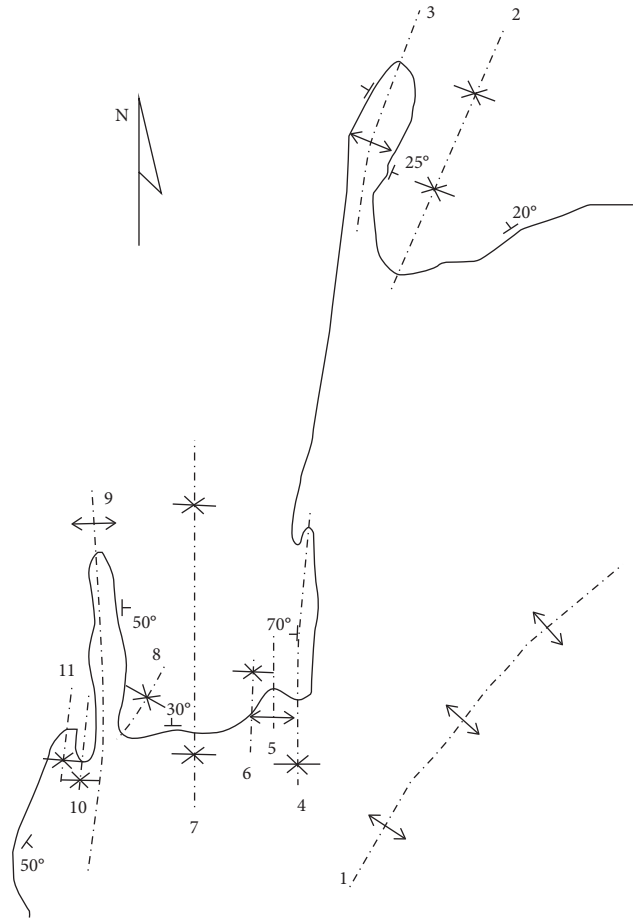


Figure 24: Tectonic outline map of the Nantong Coal Mine Zone. 1, Longguxigeo anticline; 2, Conglingou syncline; 3, Xianjiaping anticline; 4, Ganjiaping syncline; 5, Maoyan anticline; 6, Yaqueyan syncline; 7, Bamianshan syncline; 8, Wangjiaba syncline; 9, Wuguishan anticline; 10, Pingtu syncline; 11, Miaoding syncline.

Table 2: Compound coal-rock dynamic disasters in Donglin Coal Mine.

| | | Parameters |
|---|---|---|
| Times | No. 4 coal seam | 152 |
| | No. 6 coal seam | 41 |
| Maximum strength (t) | No. 4 coal seam | 3500 |
| | No. 6 coal seam | 160 |

Table 3: Gas parameters of coal found by laboratory investigation.

| Sampling site | Initial gas emission velocity $\Delta P$ | Firmness coefficient of soft coal $f$ | $K_1$-$P$ relational model, $K_1 = AP^B$ | | | | | |
|---|---|---|---|---|---|---|---|---|
| | | | $A$ | $B$ | 0.50 MPa | 0.60 MPa | 0.74 MPa | 1.10 MPa |
| 2607-50 heading face | 6 | 0.27 | 0.1472 | 0.5582 | $K_1 = 0.10$ | $K_1 = 0.11$ | $K_1 = 0.12$ | $K_1 = 0.16$ |
| 2607-50 heading face | 5 | 0.26 | 0.1902 | 0.7115 | $K_1 = 0.12$ | $K_1 = 0.14$ | $K_1 = 0.15$ | $K_1 = 0.20$ |
| 2609-90 heading face | 8 | 0.29 | 0.2196 | 0.6989 | $K_1 = 0.14$ | $K_1 = 0.15$ | $K_1 = 0.18$ | $K_1 = 0.23$ |

Table 4: Prediction cycle cuttings desorption index $K_1$ with changing hole depth.

| Prediction hole depth (m) | 1 | 2 | 3 | 4 | 5 | 6 | 7 | 8 | 9 | 10 |
|---|---|---|---|---|---|---|---|---|---|---|
| Prediction times | 9 | 93 | 30 | 82 | 27 | 66 | 23 | 55 | 18 | 33 |
| $K_{1max}$ (ml/g·min$^{1/2}$) | 0.06 | 0.34 | 0.22 | 0.37 | 0.3 | 0.35 | 0.21 | 0.46 | 0.21 | 0.33 |
| $K_{1max}$ (ml/g·min$^{1/2}$) | 0.01 | 0 | 0.01 | 0 | 0.02 | 0 | 0.01 | 0.02 | 0.01 | 0 |
| Average value of $K_1$ (ml/g·min$^{1/2}$) | 0.03 | 0.08 | 0.07 | 0.08 | 0.08 | 0.07 | 0.06 | 0.07 | 0.08 | 0.07 |

Table 5: Prediction cycle drilling chip amount index $S$ with changing hole depth.

| Prediction hole depth (m) | 1 | 2 | 3 | 4 | 5 | 6 | 7 | 8 | 9 | 10 |
|---|---|---|---|---|---|---|---|---|---|---|
| Prediction times | 107 | 122 | 115 | 112 | 94 | 94 | 79 | 76 | 56 | 47 |
| $S_{max}$ (kg/m) | 18.5 | 64 | 36 | 26 | 42 | 73 | 48 | 40 | 42 | 30 |
| $S_{min}$ (kg/m) | 0.6 | 0.8 | 0.6 | 1.2 | 1.8 | 1.8 | 2.2 | 1.6 | 1 | 1.2 |
| Average value of $S$ (kg/m) | 2.4 | 3.4 | 4.8 | 4.7 | 5.6 | 7.1 | 7.7 | 7.8 | 8.2 | 7.4 |

Table 6: Prediction cycle percentage-based statistics of cuttings desorption index.

| $K_{1max}$ (ml/g·min$^{1/2}$) | Total times/58 | Percentage (%) | $S_{max}$ (kg/m) | Total times/58 | Percentage (%) |
|---|---|---|---|---|---|
| ≥0.05 | 55 | 95 | ≥6 | 42 | 72 |
| ≥0.1 | 39 | 67 | ≥10 | 27 | 47 |
| ≥0.15 | 26 | 45 | ≥12 | 23 | 40 |
| ≥0.2 | 18 | 31 | ≥15 | 16 | 28 |
| ≥0.25 | 8 | 14 | ≥20 | 12 | 21 |
| ≥0.3 | 6 | 10 | ≥25 | 9 | 16 |
| ≥0.35 | 4 | 7 | ≥30 | 7 | 12 |
| ≥0.4 | 1 | 2 | ≥35 | 1 | 2 |

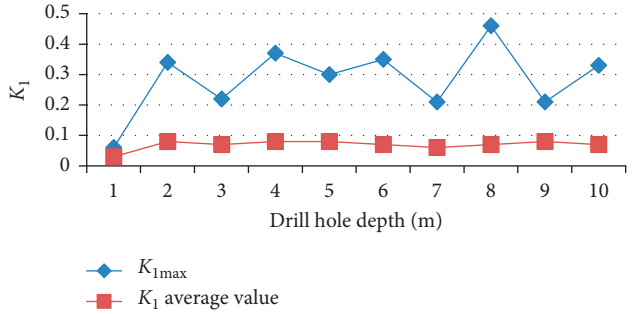


Figure 25: Distribution of 58 sets prediction cycle cuttings desorption index $K_1$ at different hole depths.

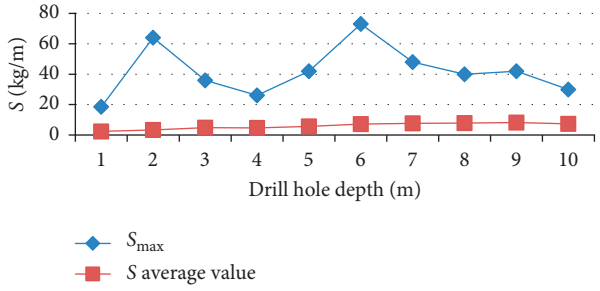


Figure 26: Distribution of 58 sets of prediction cycle drilling chip amount index $S$ at different hole depths.

maximum value of $S$ exceeding 30% is 15 kg/m, the proportion of which is 28% overall. When $S_{max}$ exceeds 15 kg/m, kinetic phenomena including drill jamming, coal-gunning, and collapse occur frequently.

*3.2.3. Prediction Index and Critical Value of the No. 6 Coal Seam of Compound Coal-Rock Dynamic Disasters in Donglin Coal Mine.* In combination with laboratory investigation, field data statistics, and field kinetic phenomena, the cuttings desorption index $K_1$ is taken as the gas prediction index, with a critical value of 0.2 mL/(g·min$^{1/2}$).

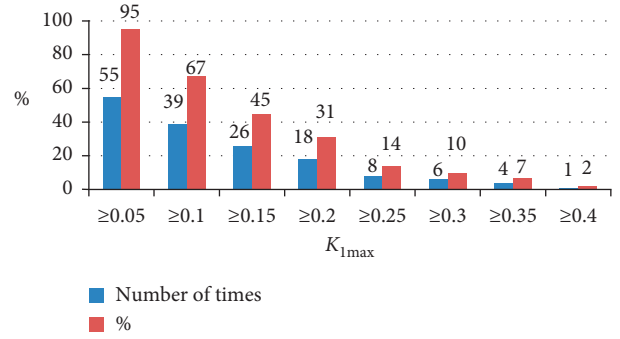


Figure 27: Distribution of 58 sets of prediction cycle cuttings desorption index $K_{1max}$.

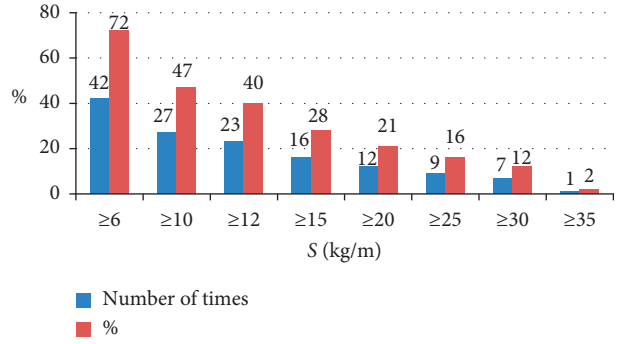


Figure 28: Distribution of 58 sets of prediction cycle drilling chip amount index $S_{1max}$.

Based on the field test data statistics and actual kinetic phenomenon, the drilling chip amount $S$ can be determined as the crustal stress index of compound coal-rock dynamic disaster for the No. 6 seam in the contorted fold structure band of Donglin Coal Mine, with a critical value of 15 kg/m.

According to these prediction indices and critical values, 85 sets of prediction data and check cycle analysis were adopted during extensive field application. During the

excavation of a 257.5 m long roadway, no compound coal-rock dynamic disaster occurred.

## 4. Conclusion

(1) The areas of occurrence of compound coal-rock dynamic disasters are those with high crustal stress confining pressure, high gas pressure, and low permeability; the coal mechanical properties of compound coal-rock dynamic disaster exhibit bump proneness and outburst risk.

(2) The gas desorption velocity and permeability reduce with the increase in crustal stress, while increase and decrease with increasing gas pressure, respectively. A temperature variation within 30°C has limited influence on the gas desorption velocity.

(3) As the mining depth increases, the crustal stress and gas pressure both increase. At the same time, compared to the gas pressure, the increase amplitude and velocity of crustal stress increase, resulting in the increase in coal strain energy, elastic modulus, bump energy index, and elastic energy index. Meanwhile, the dynamic fracture time is reduced. Gas extraction leads to the increase in bump energy index and elastic energy index, while reducing the dynamic fracture time; thus, the risk of compound coal-rock dynamic disaster is significantly increased.

(4) Based on the actual geological conditions of Donglin Coal Mine, the prediction sensitivity index and critical value of compound coal-rock dynamic disaster were investigated. The cuttings desorption index $K_1$ and drilling chip amount $S$ were set as the sensitivity index, with critical values of 0.2 mL/(g·min$^{1/2}$) and 15 kg/m, respectively.

## Data Availability

The data used to support the findings of this study are included within this article.

## Conflicts of Interest

The authors declare that there are no conflicts of interest.

## Authors' Contributions

Dong G and Wang Z conceived and designed the experiments. Wang Z performed the experiments. Wang Z and Liang X analysed the data. Dong G wrote the paper.

## Acknowledgments

This work was funded by the National Key Research and Development Programme of China (Grant no. 2016YFC0801402), National Science and Technology Major Project of the Ministry of Science and Technology of China in the 13th Five-Year Period (Grant no. 2016ZX05045-004), One Hundred Youth Talents Project of Shaanxi Province of China, Shaanxi Natural Science Foundation of China (Grant no. 2020JM-519), and the Research Fund of the State Key Laboratory of Coal Resources and Safe Mining, CUMT (Grant no. SKLCRSM18KF017).

## References

[1] I. M. Petukhov, "Theory and Practice in rock burst prevention," in *Proceedings of the 22nd International Conference on Mining Safety*, Beijing, China, 1987.

[2] M. Zhang, Z. Xu, and Y. Pan, "A united instability theory on coal (rock) burst and outburst," *Journal of China Coal Society*, vol. 16, no. 4, pp. 48–52, 1991.

[3] M. He, H. Xie, S. Peng, and Y.-D. Jiang, "Study on rock mechanics in deep mining engineering," *Chinese Journal of Rock Mechanics and Engineering*, vol. 24, no. 16, pp. 2803–2813, 2005.

[4] T. Li, M. Cai, J. Wang et al., "Discussion on relativity between rock burst and gas in deep exploitation," *Journal of China Coal Society*, vol. 30, no. 5, pp. 562–567, 2005.

[5] T. Li, T. Mei, G. Li et al., "Mechanism study of coal and gas outburst induced by rockburst in "three-soft" coal seam," *Chinese Journal of Rock Mechanics and Engineering*, vol. 30, no. 6, pp. 1283–1288, 2011.

[6] Z. Li, *Rock-Burst Mechanism and Application of High-Methane Coal-Seam*, Liaoning Technical University, Fuxin, China, 2007.

[7] H. Zhang, Jun, W. Song et al., *Geology Dynamic Division*, Coal industry Press, Beijing, China, 2009.

[8] Y.-S. Pan, "Integrated study on compound dynamic disaster of coal-gas outburst and rockburst," *Journal of China Coal Society*, vol. 41, no. 1, pp. 105–112, 2016.

[9] G. Yin, L. Xing, J. Lu, and M. Li, "Disaster-causing mechanism of compound dynamic disaster in deep mining under static and dynamic load conditions," *Journal of China Coal Society*, vol. 42, no. 9, pp. 2316–2326, 2017.

[10] L. Dou, X. He, T. Ren et al., "Mechanism of coal-gas dynamic disasters caused by the superposition of static and dynamic loads and its control technology," *Journal of China University of Mining & Technology*, vol. 47, no. 1, pp. 48–59, 2018.

[11] G. Dong, H. Jin, Q. Hu et al., *Compound Coal-Rock Dynamic Disaster Forecasting and Early Warning and its Application*, China University of Mining and Technology Press, Xuzhou, China, 2017.

[12] F. Zhang and T. Li, "Cognizance on compound dynamic disaster of coal and gas in deep mining," *Zhongzhou Coal*, vol. 4, pp. 73–76, 2009.

[13] W. Zhen, Y. Guangzhi, H. Qianting et al., "Study on induced transformation conditions of rock burst and outburst in high gassy seams," *Journal of Mining and Safety Engineering*, vol. 27, no. 4, pp. 572–580, 2010.

[14] H. Li, J. Han, Z. Xiong et al., "Analysis and prevention of complex dynamic phenomena in deep mining," *Coal Engineering*, vol. 7, no. 4, pp. 40-41, 2010.

[15] R. Yuan, "Features of dynamic disasters combined rockburst and gas outburst in deep coal mine and its preventive measures," *Coal Science and Technology*, vol. 47, no. 8, pp. 6–10, 2013.

[16] H. Li, L. Qi, X. Chen et al., "The influence of gas pressure on mobile mechanism of coal rock burst," *Safety in Coal Mines*, vol. 44, no. 9, pp. 1–4, 2013.

[17] L. Qi, X. Chen, G. Cheng et al., "Research on the burst triggering mechanism under the coupling action of higher stress and gas pressure," *Journal of North China Institute of Sci-Ence and Technology*, vol. 11, no. 2, pp. 18–21, 2014.

[18] T.-G. Zhang, "Prediction and control of coal and gas outburst in Pingdingshan Mining Area," *Journal of China Coal Society*, vol. 26, no. 2, pp. 172–177, 2001.

[19] G. Jianwei, *Hazard Assessment and Monitoring Technology of Com-Pound Dynamic Disaster in Mine*, China University of Mining and Technology, Xuzhou, China, 2013.
[20] F. Jiang, G. Yang, W. Quande et al., "Study and prospect on coal mine composite dynamic disaster real-time prewarning platform," *Journal of China Coal Society*, vol. 43, no. 2, pp. 333–339, 2018.
[21] L. Sheng, H. Yang, M. Luo et al., "Improved comprehensive index evaluation method and its application on rockburst hazard of gas coal seam," *Coal Science and Technology*, vol. 13, no. 11, pp. 34–40, 2017.
[22] Z. Ouyang, G. Zhang, H. Qin et al., "Improved comprehensive index evaluation method and its application on rockburst hazard of gas coal seam," *Coal Science and Technology*, vol. 46, no. 10, pp. 30–36, 2018.
[23] Q. Qi, Y. Pan, L. Shu et al., "Theory and technical framework of prevention and control with different sources in multi-scales for coal and rock dynamic in deep mining of coal mines," *Journal of China Coal Society*, vol. 43, no. 7, pp. 1801–1810, 2018.
[24] C. Wang, X. Li, C. Xu et al., "Study on factors influencing and the critical value of the drilling cuttings weight: an index for outburst risk prediction," *Process Safety and Environmental Protection*, vol. 140, pp. 356–366, 2020.
[25] C.-P. Lu, G.-J. Liu, Y. Liu, N. Zhang, J.-H. Xue, and L. Zhang, "Microseismic multi-parameter characteristics of rockburst hazard induced by hard roof fall and high stress concentration," *International Journal of Rock Mechanics and Mining Sciences*, vol. 76, pp. 18–32, 2015.
[26] G. Dong, X. Ren, and Z. Wang, "A novel early warning method for atypical outbursts disasters in mines: extraction of indexes from gas concentration data for the early warning of atypical outbursts," *Arabian Journal of Geosciences*, vol. 12, no. 24, p. 796, 2019.